NRC Research Press

ARTICLE

Morphological instability at the solid–liquid interface by the maximum entropy production rate principle

Yaw Delali Bensah

Abstract: We examine the morphological instability from planar to non-planar cellular morphology with the maximum entropy production rate (MEPR) principle. An expression that quantifies the MEPR density at the solid–liquid interface (SLI) during direction solidification is presented, which leads to an instability criterion for dilute binary alloys. The instability criterion also affords to theoretically calculate the instability solidification growth velocity. The model considers steady state solidification at close-to and far-from equilibrium conditions.

Key words: maximum entropy production rate (MEPR) principle, planar morphology, cellular morphology, morphological transition, solid–liquid interface.

Résumé : Nous utilisons le principe du taux maximum de production d'entropie (TMPE) pour examiner l'instabilité morphologique, passant de morphologie cellulaire planaire à non planaire. Nous présentons une expression qui quantifie la densité du TMPE à l'interface solide–liquide (ISL) durant la solidification directionnelle et qui mène à un critère d'instabilité pour les alliages binaires dilués. Ce critère d'instabilité permet aussi le calcul théorique de la vitesse de croissance de la solidification en instabilité. Le modèle considère la solidification stationnaire sous des conditions proches et éloignées des conditions d'équilibre. [Traduit par la Rédaction]

Mots-clés : principe du taux maximum de production d'entropie, transition morphologique, morphologie cellulaire, morphologie planaire, interface solide–liquide.

1. Introduction

When an alloy melt is directionally solidified, a planar morphology is first noted at the solid-liquid interface (SLI), usually at a very low velocity of transformation. As the velocity is increased (e.g., either by increasing the cooling rate or the solidification growth rate), the planar interface becomes unstable to other shapes and transforms to a macroscopically jagged or wavy cellular morphology with several variations in topography [1]. When a planar to non-planar topographical transition occurs during solidification, it is expected to be a consequence of a thermodynamic driving force and the new shape formed provides stability compared to other shapes [2]. This morphological instability was first studied for a sharp interface condition by Tiller et al. [3] under the constitutional undercooling theory (CUT) and later by Mullins and Sekerka [4] under the linear stability theory (LST). A sharp interface is when there is no density change at the interface between the fully liquid and the fully solid (i.e., the free energy change with respect to density is zero). At instability, the CUT and LST are described by

$$\left(\frac{V}{G_L}\right)_C = \frac{D_L}{\Delta T_O} \tag{1}$$

$$\left(\frac{V}{G_L}\right)_C = \frac{D_L}{\Delta T_O}\frac{2K_L}{(K_S + K_L)S} \tag{2}$$

respectively, where V (m s^{-1}) is the solidification growth velocity, G_L (K m^{-1}) is the temperature gradient in the liquid, D_L (m^2 s^{-1}) is the solute diffusion coefficient in the liquid, and ΔT_O (K) is the equilibrium solidification range ($T_l - T_S$) for a liquid at composition C_O (mol m^{-3}). Also T_l (K) and T_S (K) are the equilibrium liquidus and solidus temperatures that are measured from the phase diagram. Also, S (no units) is Mullins and Sekerka stability constant [4], which is approximately equal to one for low velocities and, K_L and K_S (J m^{-1} K^{-1} s^{-1}) are the thermal conductivities for the rigorous solid and liquid, respectively. The subscript "$_C$" refers to the critical condition for instability.

The CUT and LST models converge for the limit where K_L approaches K_S.

The same problem has been studied for a diffuse interface (DI) condition by Cahn [5, 6] using a near equilibrium thermodynamic approach and by Sekhar [2] using the maximum entropy production rate (MEPR) principle. A DI is considered when there is a defined gap between the fully liquid and the fully formed solid. It considers a free energy change with respect to density to be greater than zero.

Generally, the MEPR is an extremum thermodynamic principle, which was first proposed by Ziman [7] and later echoed by Jaynes [8], with its rigorous theoretical foundation laid by Ziegler [9, 10]. The principle has also seen major theoretical exposition and expansion by Dewar [11], and by Martyushev and Seleznev [12].

Generally, modelling of complex systems and formulation of dynamical equations in sufficient detail are difficult and often could be problematic [13], but MEPR has been of considerable utility [14–17]. The role of MEPR is to take the place of the dynamics in such formulations [13] with applications to linear and nonlinear thermodynamics [9, 10]. According to MEPR, a non-equilibrium system subject

Received 9 November 2017. Accepted 3 April 2018.

Y.D. Bensah. Department of Materials Science and Engineering, University of Ghana, Accra, Ghana.
Email for correspondence: ydbensah@ug.edu.gh.

to perturbations of sufficiently large amplitude selects a state characterized by MEPR [2, 12]. The MEPR principle has been further considered for self-organizing behavior in chemical reactions [18], Belousov–Zhabotinsky type reactions [2, 19], complex biochemical reactions [20, 21], and climatology [22].

In the field of solidification and crystal growth, MEPR has been used to study the morphological instability and curvature in nonequilibrium systems [2, 23–25]. In their seminal paper, Sekhar [2] showed that the MEPR principle considers that entropy generation occurs in all irreversible processes and become maximized as a way of determining its pathway. Sekhar used well-known concepts to find a connection between entropy and key material properties relevant to directional solidification (DS) of the Bridgman type, and showed that for a control volume (i.e., the SLI in diffuse form) the entropy generation rate density $\dot{s}_E$(J m^{-3} K^{-1} s^{-1}), which describes the new entropy generated due to exchange of matter at the SLI, is given as

$$\dot{s}_E = \frac{VG_{SLI}}{\Delta T_{SLI}}\left(\frac{\Delta h_{sl}T_{li} - \Delta h_m T_{si}}{T_{si}T_{li}}\right) \tag{3a}$$

where Δh_{sl} (J m^{-3}) is the heat of fusion; T_{li} (K) and T_{si} (K) are liquidus and solidus temperatures, respectively, at the SLI boundaries; G_{SLI} (K m^{-1}) is the linear temperature gradient across the SLI; and ΔT_{SLI} (K) is the difference between T_{li} and T_{si}. Sekhar showed that the heat of fusion of the solid with defects, Δh_m (J m^{-3}), and the heat of fusion, Δh_{sl}, are related by $\Delta h_{sl} = \Delta h_m + \omega_D$, where ω_D (J m^{-3}) is the energy of defects (such as grain boundaries or dislocations) per unit volume. Sekhar assumed that ω_D is a relatively small term compared to Δh_m and therefore could be simplified as $\Delta h_{sl} = \Delta h_m$. Also, T_{li} and T_{si} are not readily known, but for dilute binary materials they can be approximated to be equal to the melting temperature, T_M (K). From this, then (3*a*) can be simplified as

$$\dot{s}_E = \frac{V\Delta h_{sl}G_{SLI}}{T_M^2} \tag{3b}$$

Sekhar further showed that within the liquid melt the entropy rate density, which describes the force-flux entropy generated by the existence and maintenance of solute gradient, is [2]

$$\dot{s}_{LG} = \frac{\Delta T_O}{D_L}\frac{V^2R_g\ln(1/k)}{4m_L} \tag{4}$$

where R_g (J mol^{-1} K^{-1}) is the molar gas constant, k (no units) is the partition coefficient that can be obtained from the binary phase diagram, and m_L (K m^3 mol^{-1}) is the slope of the liquidus line at the solid–liquid boundary for a binary material. It should be noted that (4) is slightly modified and simplified from the original terse derivation by Sekhar. An expanded derivation of (4) is given in Appendix A.

In spite of the advances made by Sekhar, they inaccurately assumed (3) to be equivalent to the maximum entropy generation rate density for binary alloys, which leads to morphological instability criterion, as

$$V\delta_C \cong 2D_L \tag{5}$$

Using (5) as basis, they linked (3) and (4) to obtain an approximated instability solidification growth velocity as given in

$$\left(\frac{V}{G_{SLI}}\right)_C = 4\left(\frac{\Delta S_{sl}}{R}\right)\left[\frac{1}{(1-k)}\right]\frac{D_L}{\Delta T_O} \tag{6}$$

where δ_C (m) is the solute boundary layer, R (J m^{-3} K^{-1}) is the volumetric gas constant, and ΔS_{sl} (J m^{-3} K^{-1}) is the entropy change during solidification per unit volume.

Despite the progress made by Sekhar, it is worth noting that (5), which is the instability criterion, has a weak dependence on MEPR. Furthermore, the consideration of (3*b*) as a measure of MEPR is not entirely correct for the case of binary alloys.

In this article, we take a step further beyond Sekhar's MEPR theory and develop an expression for the maximum entropy generation rate density ($\dot{\varphi}_{max}$) as a measure of MEPR at the SLI in the case of DS for binary alloys. Through an entropy balance approach we establish a connection between the maximum entropy generation rate density and the other forms of entropy developed by Sekhar in (3) and (4). From the entropy balance expression we arrive at an instability criterion and a new expression for calculating solidification growth velocity at the critical condition for binary metal and non-metal alloys. The results are compared with that of CUT and LST.

2. Method

2.1. Model and entropy generation at the SLI

Consider the changeover region between a solidifying liquid to solid in DS system that has a finite dimension over which a temperature gradient and other gradients are established. This changeover zone is called a SLI region with a thickness ζ (m). The SLI is considered diffuse (or a DI) because it contains a mix of rigorous liquid and solid (crystals). The entropy rate balance for the control volume is given by [2]

$$\frac{ds_{cv}}{dt} = \dot{s}_{in} - \dot{s}_{out} + \dot{s}_{gen} \tag{7}$$

where ds_{CV}/dt (J m^{-3} K^{-1} s^{-1}) is the total steady state entropy rate change in the control volume; $\dot{s}_{in}$ (J m^{-3} K^{-1} s^{-1}) and $\dot{s}_{out}$ (J m^{-3} K^{-1} s^{-1}) are the rate of entropy entering and leaving the control volume, respectively; and $\dot{s}_{gen}$ (J m^{-3} K^{-1} s^{-1}) is the irreversible entropy generation rate in the SLI region. The rates of entropy entering ($\dot{s}_{in}$) and leaving ($\dot{s}_{out}$) the control volume are, respectively, given by

$$\dot{s}_{in} = \frac{V}{\zeta}\left(\frac{\Delta h_{sl}}{T_{li}} + s_{LG} + s_{SG}\right) \tag{8}$$

$$\dot{s}_{out} = \frac{V}{\zeta}\left(\frac{\Delta h_m}{T_{si}} + s_{SG}\right) \tag{9}$$

where the subscripts ($_{LG}$) and ($_{SG}$) refer to solute gradients in the liquid and solid, respectively; s_{LG} (J m^{-3} K^{-1}) is the entropy generation density due to solute gradient in the liquid; and s_{SG} (J m^{-3} K^{-1}) is the entropy generation density due to solute gradient in the solid. Combining (8) and (9) into (7) yields the control volume expression at steady state as

$$\frac{ds_{cv}}{dt} = \dot{s}_E + \dot{s}_{LG} + \dot{s}_{gen} \tag{10}$$

where $\dot{s}_{LG}$ (J m^{-3} K^{-1} s^{-1}) is the entropy generation rate density by the solute gradient in the liquid. Applying the steady state condition ($ds_{cv}/dt = 0$) to (10), then the total entropy generation rate density at the interface (i.e., the SLI region) becomes

$$\dot{s}_{gen} = \dot{s}_E - \dot{s}_{LG} \tag{11a}$$

If we consider that the morphological transition from a plane front to a cellular shape occurs when $\dot{s}_{gen}$ reaches a maximum then, $\dot{s}_{gen} \cong \dot{\varphi}_{max}$, and (11*a*) becomes

$$\dot{\varphi}_{max} = \dot{s}_E - \dot{s}_{LG} \tag{11b}$$

The key hypothesis in this article is that MEPR is operative with maximum entropy generation rate density, $\dot{\varphi}_{max}$ (J m^{-3} K^{-1} s^{-1}), within the SLI, which has the capability of predicting the most stable morphology. In Subsect. 2.2 we derive an expression for the maximum entropy generation rate density ($\dot{\varphi}_{max}$).

2.2. Entropy generation and the conversion of kinetic energy

By the definition of the SLI established, we consider the motion of the SLI during DS as a single unit of mass and not as individual mass of atomic particles or crystalline particles with velocity equal to the solidification growth velocity. The overall transformation from liquid to solid includes a density change given by

$$|\Delta\rho_k| = \left|\frac{\rho_l \Delta\rho}{\rho_s}\right| \tag{12}$$

where $|\Delta\rho_k|$ (kg m^{-3}) is the overall density shrinkage; $\Delta\rho$ (kg m^{-3}) is the density change from liquid to solid ($\rho_s - \rho_l$); and ρ_s (kg m^{-3}) and ρ_l (kg m^{-3}) are the densities of rigorous solid and liquid, respectively. For the rest of this derivation the modulus sign for the density shrinkage is omitted. The volume shrinkage $\Delta\Omega_S$ (m^3) associated with the liquid to solid transformation is given as

$$\Delta\Omega_S = A_{SLI}\zeta\Delta\rho_k \tag{13}$$

where A_{SLI} (m^2) is the area of the SLI. The associated change in kinetic energy of the moving liquid transforming into the solid is expressed as

$$\Delta KE = \frac{1}{2}\rho_l \Delta\Omega_S V^2 \tag{14}$$

Placing (12) and (13) into (14) gives the overall gain or loss in kinetic energy ΔKE (J) of the transforming liquid entering into the SLI as

$$\Delta KE = \frac{A_{SLI}\zeta\Delta\rho_k V^2}{2} \tag{15}$$

The moving interface dissipates free energy equal to the lost work, W_L (J), as given in [9]

$$W_L = T_{av}(S_{gen})_{max} \tag{16}$$

We consider that the lost work is equivalent to the loss in kinetic energy given in

$$(S_{gen})_{max} = \frac{A_{SLI}\zeta\Delta\rho_k V^2}{2T_{av}} \tag{17}$$

which is obtained by combining (15) and (16). Here $(S_{gen})_{max}$ (J K^{-1}) is the maximum entropy generation due to the lost work and T_{av} (K) is the average temperature between T_{li} and T_{si} across the SLI.

Following the work term introduced in (16), the main assumption in this article is that the loss in kinetic energy is converted to heat, which is further converted to some work subject now to the limitation of the second law of thermodynamics. The heat generation Q (J) from the conversion of the loss in kinetic energy is given as

$$Q = A_{SLI}\zeta C_p \Delta T_{SLI} \tag{18}$$

where C_p (J m^{-3} K^{-1}) is the average heat capacity across the SLI. Equation (18) is the equivalence of the lost work potential from the heat generation. With (16), the equivalent entropy generation through heat dissipation, $(S_{gen})_{HD}$ (J K^{-1}) may be approximated as

$$(S_{gen})_{HD} = A_{SLI}\zeta C_p \frac{\Delta T_{SLI}}{T_{av}} \tag{19}$$

where the subscript ($_{HD}$) indicates the heat dissipation. The temperature gradient at the SLI (G_{SLI}) maybe approximated as

$$G_{SLI} = \frac{(G_S + G_L)}{2} \tag{20}$$

where G_S (K m^{-1}) is the temperature gradient in the solid. The maximum entropy generation due to the lost work is equal to the equivalent entropy generation through heat dissipation.

It is also assumed that the thermal gradient (similar to assumptions made in the linear stability model [4]) across the SLI is linear and expressed as

$$\Delta T_{SLI} = T_{li} - T_{si} = \zeta G_{SLI} \tag{21}$$

Combining (17) and (19) and substituting in (21) and (20) gives the heat capacity

$$C_p = \frac{\Delta\rho_k V^2}{2\zeta G_{SLI}} \tag{22}$$

The maximum entropy generation rate density (MEPR), $\dot{\varphi}_{max}$ (J m^{-3} K^{-1} s^{-1}), is now obtained by multiplying (22) by the change in the fraction of the liquid solidified per second

$$\frac{df_s}{dt} = \frac{V}{\zeta} \tag{23}$$

$$\left(C_p \frac{df_s}{dt}\right)_{max} = \frac{d\varphi_{max}}{dt} = \dot{\varphi}_{max} \tag{24a}$$

$$\dot{\varphi}_{max} = \frac{\Delta\rho_k V^3}{2\zeta^2 G_{SLI}} \tag{24b}$$

where f_s (dimensionless) is the fraction solidified and t (s) is time. Thus $\dot{\varphi}_{max}$ becomes a function of ζ, V, and G_{SLI}. When partitioning is feasible, the maximum entropy generated rate density can be expressed by combining (3*b*), (4), and (24*b*) into (11*b*) as

$$\dot{\varphi}_{max} = \frac{V\Delta h_{sl} G_{SLI}}{T_{li}T_{si}} - \frac{\Delta T_O}{D_L}\frac{V^2 R_g \ln(1/k)}{4m_L} \tag{25}$$

The maximization of the entropy generation rate (25) is the pathway for the selection that the interface will prefer.

Table 1. Data and physical constant used.

Binary material	G_L (K m^{-1})	D_L (×10^{-9} m^2 s^{-1}) at T_S	T_s (K)	T_l (K)	k (no units)	Δh_{sl} (J m^{-3})	K_S (J m^{-1} K^{-1} s^{-1})	K_L (J m^{-1} K^{-1} s^{-1})	T_M (K)
Al-0.102 wt%Cr	1610	0.261	933.81	933.88	1.33	9.25×10^8	247	94.05	933.60
Al-0.201 wt%Cr	2300	0.261	934.01	934.15	1.33	9.25×10^8	247	94.05	933.60
Al-0.328 wt%Cr	3050	0.262	934.27	934.49	1.33	9.25×10^8	247	94.05	933.60
Al-0.025 wt%Cu	920	7.452	932.93	933.54	0.094	9.25×10^8	247	94.05	933.60
Al-0.47 wt%Cu	1450	7.147	920.86	932.41	0.094	9.25×10^8	247	94.05	933.60
Al-0.20 wt%Cu	2500	7.332	928.19	933.09	0.094	9.25×10^8	247	94.05	933.60
Al-0.73 wt%Cu	2000	6.971	913.78	931.74	0.094	9.25×10^8	247	94.05	933.60
Al-0.083 wt%Zn	970	4.442	933.31	933.48	0.41	9.25×10^8	247	94.05	933.60
Al-0.096 wt%Zn	2650	4.439	933.26	933.46	0.41	9.25×10^8	247	94.05	933.60
Al-0.375 wt%Zn	1310	4.398	932.26	933.05	0.41	9.25×10^8	247	94.05	933.60
Pb-0.01 wt%Sn	540	1.656	600.60	600.62	0.636	2.48×10^8	33.6	15.4	600.65
Pb-0.03 wt%Sn	820	1.655	600.51	600.56	0.636	2.48×10^8	33.6	15.4	600.65
Pb-0.05 wt%Sn	1380	1.654	600.41	600.49	0.636	2.48×10^8	33.6	15.4	600.65
Pb-0.06 wt%Sn	1220	1.653	600.36	600.47	0.636	2.48×10^8	33.6	15.4	600.65
Pb-0.1 wt%Sn	1200	1.652	600.17	600.35	0.636	2.48×10^8	33.6	15.4	600.65
Pb-0.15 wt%Sn	1300	1.649	599.93	600.19	0.636	2.48×10^8	33.6	15.4	600.65
SCN-0.7 wt% Sal	3800	0.685	328.57	330.76	0.18	4.57×10^7	0.225	0.223	331.25
SCN-0.5 wt% Sal	10000	0.904	329.34	330.90	0.18	4.57×10^7	0.225	0.223	331.25
SCN-0.5 wt% Ace	2400	9.681	314.24	329.53	0.101	4.57×10^7	0.225	0.223	331.25
SCN-0.1 wt% Ace	6500	1.455	327.84	330.91	0.101	4.57×10^7	0.225	0.223	331.25
SCN-0.165 wt% Ace	1700	3.039	330.68	325.63	0.101	4.57×10^7	0.225	0.223	331.25
SCN-0.106 wt% Ace	3800	1.102	327.64	330.89	0.101	4.57×10^7	0.225	0.223	331.25

Note: Experimental data is individually referenced in [1]. G_{SLI} was assumed to be equal to G_L for (26).

Table 2. A summary of results for V/G_L at instability conditions for experimental breakdown compared with the current MEPR criterion and other instability theories.

	$(V/G_L)_C$ at breakdown (× 10^{-9} m^2 K^{-1} s^{-1})					Percent deviation from expt			
Binary material	Expt	Current MEPR	CUT	LST	Sekhar theory	Current MEPR	CUT	LST	Sekhar theory
Al-0.102 wt%Cr	24.596	9.269	3.791	2.091	62.21	24.64	84.59	91.50	60.46
Al-0.201 wt%Cr	11.565	4.717	1.928	1.063	31.63	18.47	83.33	90.81	63.44
Al-0.328 wt%Cr	7.541	2.901	1.184	0.653	19.43	23.13	84.30	91.34	61.19
Al-0.025 wt%Cu	23.913	7.839	12.166	6.709	72.44	67.22	49.12	71.94	66.99
Al-0.47 wt%Cu	12.069	0.399	0.619	0.341	3.69	96.69	94.87	97.17	227.07
Al-0.20 wt%Cu	4.8	0.963	1.495	0.824	8.89	79.92	68.85	82.83	46.01
Al-0.73 wt%Cu	1.1	0.250	0.388	0.214	2.31	77.18	64.73	80.55	52.38
Al-0.083 wt%Zn	37.835	25.862	25.444	14.033	232.88	31.65	32.75	62.91	83.75
Al-0.096 wt%Zn	24.868	22.349	21.987	12.127	201.24	10.13	11.59	51.23	87.64
Al-0.375 wt%Zn	6.526	5.654	5.567	3.070	50.95	13.36	14.70	52.96	87.19
Pb-0.01 wt%Sn	309.259	110.861	94.862	59.628	1005.15	64.15	69.33	80.72	69.23
Pb-0.03 wt%Sn	89.634	36.951	31.608	19.868	334.92	58.78	64.74	77.83	73.24
Pb-0.05 wt%Sn	53.261	22.169	18.958	11.916	200.87	58.38	64.41	77.63	73.48
Pb-0.06 wt%Sn	61.475	18.474	15.795	9.928	167.36	69.95	74.31	83.85	63.27
Pb-0.1 wt%Sn	47.250	11.083	9.469	5.952	100.34	76.54	79.96	87.40	52.91
Pb-0.15 wt%Sn	25.615	7.387	6.307	3.964	66.83	71.16	75.38	84.52	61.67
SCN-0.7 wt% Sal	0.589	0.267	0.312	0.311	2.05	54.67	47.03	47.20	71.27
SCN-0.5 wt% Sal	1.087	0.494	0.577	0.575	3.79	54.55	46.92	47.10	71.32
SCN-0.5 wt% Ace	0.833	0.396	0.633	0.630	3.79	52.46	24.01	24.37	78.02
SCN-0.1 wt% Ace	0.600	0.297	0.475	0.473	2.84	50.50	20.83	21.17	78.87
SCN-0.165 wt% Ace	0.765	0.376	0.602	0.599	3.60	50.85	21.31	21.70	78.75
SCN-0.106 wt% Ace	0.429	0.212	0.339	0.338	2.03	50.58	20.98	21.21	78.87

Note: The deviation from experimental results is given for each theory.

2.3. Morphological instability for a non-planar interface

We hypothesized that the onset of instability occurs only at the peak of the parabolic expression in (25) when $\dot{\varphi}_{max}$ is graphed against the velocity. That is, the MEPR instability criterion is mathematically expressed as

$$\left(\frac{\partial \dot{\varphi}_{max}}{\partial V}\right)_{\zeta, C_O} = 0 \tag{26}$$

Equation (26) is valid at the peak of $\dot{\varphi}_{max}$ against velocity. By taking the partial derivative of the maximum entropy generation rate density with respect to the velocity while holding ζ and C_O constant gives

$$\left(\frac{\partial \dot{\varphi}_{max}}{\partial V}\right)_{\zeta, C_O} = \frac{\Delta h_{sl} G_{SLI}}{T_{li} T_{si}} - \frac{\Delta T_O}{D_L} \frac{V R_g \ln(1/k)}{4 m_L} \tag{27}$$

Note that $(\partial^2 \dot{\varphi}_{max}/\partial V^2)_{\zeta, C_O}$ is negative for a maximization condition. From (26) and (27), the ratio of velocity to that of the temperature gradient is given by

$$\left(\frac{V}{G_{SLI}}\right)_C = \frac{D_L}{\Delta T_O} \frac{2 m_L \Delta h_{sl}}{T_m^2 R_g \ln(1/k)} \tag{28}$$

Fig. 1. Model prediction of calculated maximum entropy generation rate density $\dot{\varphi}_{max}$ (J m^{-3} K^{-1} s^{-1}) against V/G_{SLI} as per (25) for a number of binary materials. At the peak of the curve is the instability criterion described by (26). [Colour online.]

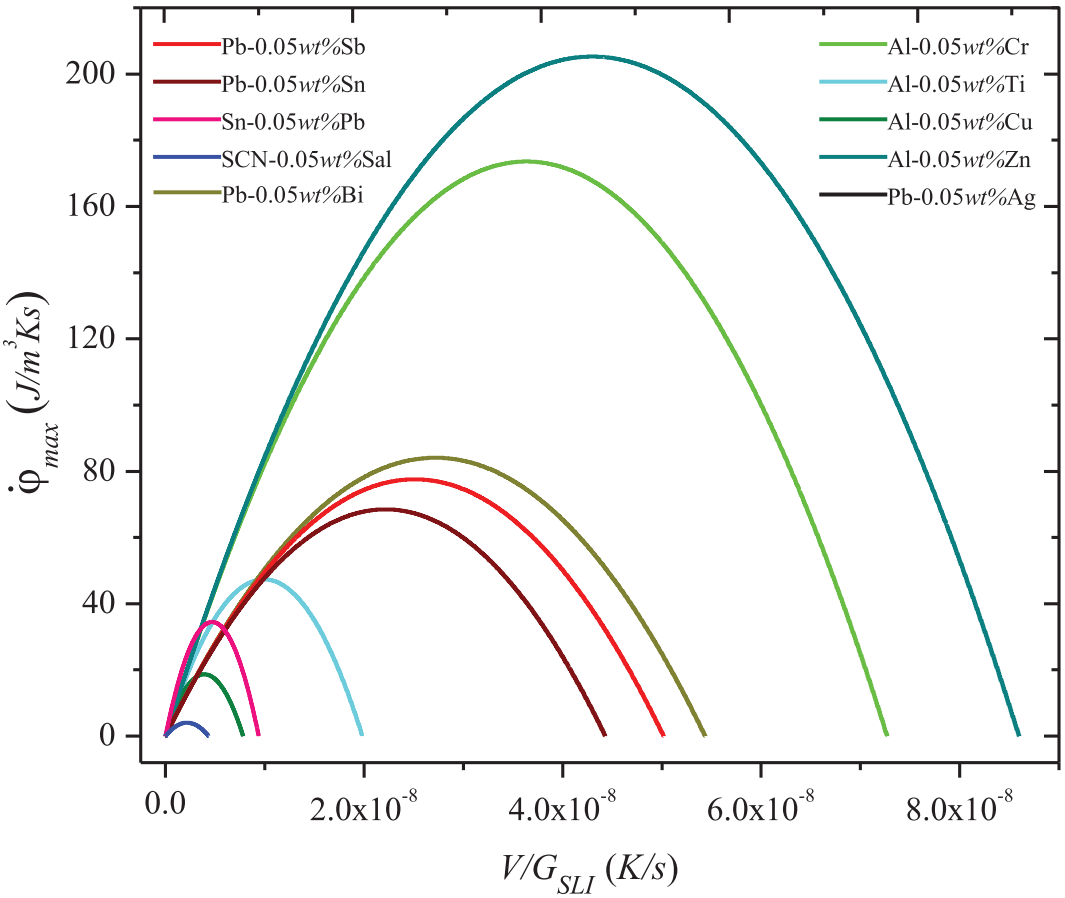

The expression given in (28) enables the prediction of the V/G_{SLI} ratio when the partition coefficient measured from the phase diagram is used.

3. Results and discussion

We have derived an expression to quantify the MEPR for a binary alloy system, which is the maximum entropy generation rate density ($\dot{\varphi}_{max}$), as given in (24). If the solidification growth velocity and the interface thickness are known, then it means $\dot{\varphi}_{max}$ will contain all information needed to select a pathway that leads to a maximization of entropy generated and as such will lead to a morphological instability (see Table 1 for data and physical constants used).

The value for $\dot{\varphi}_{max}$ cannot be less than zero because it is subject to the limitations of the second law of thermodynamics as shown in (16). This implies that regardless of the sign of G_{SLI}, the critical $\dot{\varphi}_{max}$ can only have minimum value of zero even for a planar interface and at a zero solidification growth velocity. Thus a non-planar shape can always overtake a plane front morphology for a negative temperature gradient or in other words $G_{SLI} < 0$ will always imply a breakdown into cells or other patterns. Additionally, because cellular shapes are seemingly restricted by the bounds of entropy, any other shape that offers an additional configurational entropy production rate increase because of complex features (e.g., dendrites) will always emerge unless a wide DI is formed.

When solute partitioning is possible, the entropy rate generation rate density term indicates a maximum, when plotted as a function of velocity (25). As long as no other interface configuration is feasible (ones that display a higher entropy rate generation, e.g., a jagged interface), the interface will remain planar during growth. The instability criterion given in (26) enables the prediction of the V/G_{SLI} ratio derived under (26). The V/G_{SLI} ratio calculated from the MEPR criterion is compared with experimental data for a number of binary alloy materials, as shown in Table 2. Refer to Table 1 for all the physical constants used for the results in Table 2. The computed V/G_{SLI} ratio from the current MEPR criterion generally shows a much better agreement and close match with the experimental data as compared to the CUT, LST, and Sekhar's MEPR criterion. It is important to note that the predictive capability of the CUT is much more reliable than the LST at instability. The deviation of the current MEPR results from that of experiment is mainly due to the near equilibrium assumption used in the derivation of (4) particularly, the use of the equilibrium partition coefficient as an approximation of the effectively partition coefficient for the case of a non-equilibrium system like a steady state DS process. Also the much wider deviation of Sekhar's theory is mainly due to the over approximation of (6).

The model prediction in Fig. 1 shows the relationship between the calculated maximum entropy generation rate density and V/G_{SLI}, for different classes of binary materials, which displays a typical symmetric parabolic profile. The maximum entropy generation rate density reaches a peak value and falls because the solute gradient in the liquid region begins to create new entropy compared to the amount being created by the exchange of matter across the SLI. Figure 2 shows the symmetric parabolic profile for Al–Cu at varying copper concentration. At very dilute copper con-

Fig. 2. Model prediction of calculated $\dot{\varphi}_{max}$ (J m^{-3} K^{-1} s^{-1}) against the V/G_{SLI} as per (25) for Al–Cu at different solute concentrations. The $\dot{\varphi}_{max}$ increases with decreasing solute concentration. At very low solute concentration the binary material behaves like a pure material and $\dot{\varphi}_{max}$ increases indefinitely with V/G_{SLI} ratio as a result of the partition coefficient approaching one. [Colour online.]

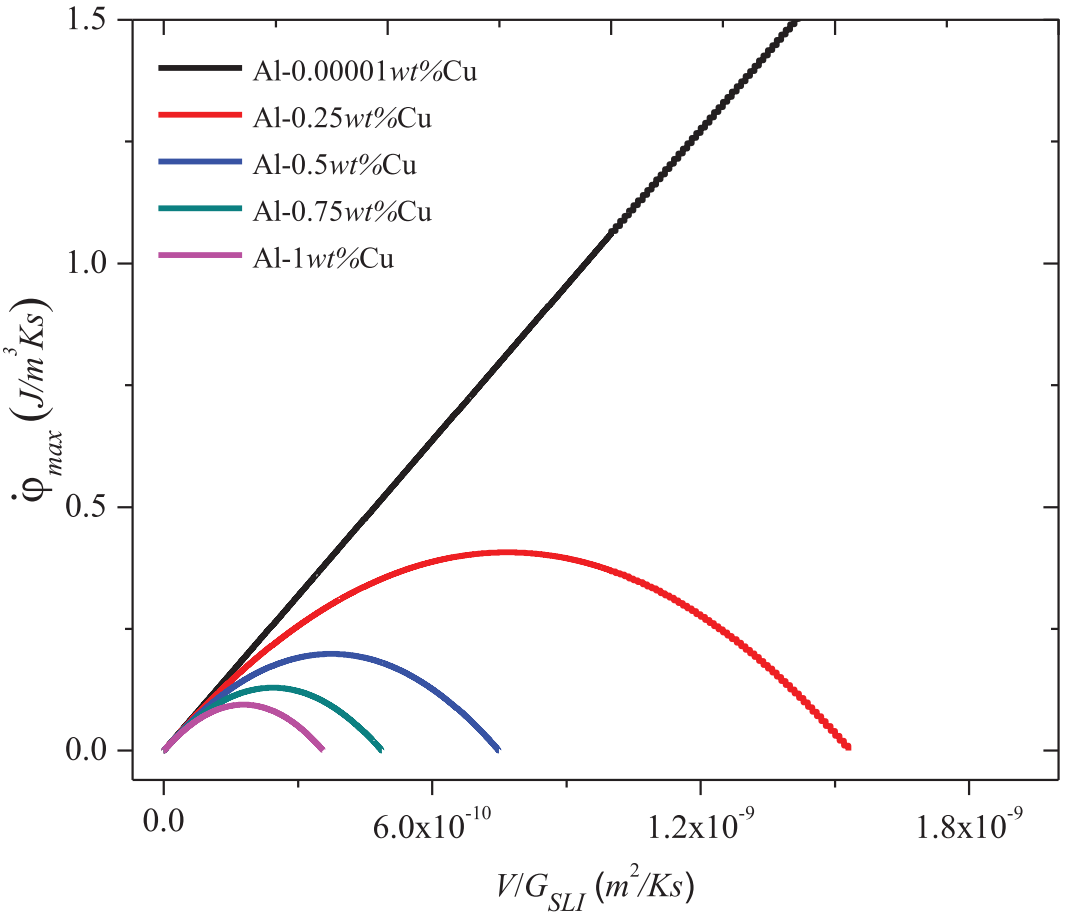

centration (Al-0.00001 wt% Cu) an indefinitely increasing entropy generation with a linear relationship to V/G_{SLI} is observed. This implies that the Al–Cu alloy is approaching that of a pure material.

4. Summary and conclusions

The key MEPR condition for SLI topographical change and breakdown is primarily as a result of the maximization entropy rate density at the SLI. It is thus related to the solidification growth velocity and the temperature gradient encountered in the solid–liquid zone, the composition, and partition coefficient when a solute gradient in the liquid is established. The MEPR model postulates that that entropy generation is maximized when an interface transition occurs to a different configuration of a topographical variant. The model for binary materials is able to quantitatively predict the critical solidification growth velocity from plane front to cellular morphology. A comparison of the critical solidification growth velocity from the MEPR criterion with that of experimentally measured data for a number of binary materials shows a good match. Furthermore, a comparison of the results obtained show that the current MEPR approach to studying instability of SLI is more reliable than the traditionally known CUT and LST approaches.

Acknowledgements

This article partly summarizes research performed for the Ph.D. award for Yaw Delali Bensah. Funding for the research came from personal savings and partial support from MHI Inc. Cincinnati, Ohio, USA. A partial tuition scholarship support received from University of Cincinnati, Cincinnati, Ohio, is acknowledged.

References

1. Y.D. Bensah and J.A. Sekhar. Curr. Opin. Chem. Eng. **3**, 91 (2014). doi:10.1016/j.coche.2013.11.005.
2. J.A. Sekhar. J. Mater. Sci. **46**, 6172 (2011). doi:10.1007/s10853-011-5688-0.
3. W.A. Tiller, K.A. Jackson, J.W. Rutter, and B. Chalmers. Acta Metall. **1**, 428 (1953). doi:10.1016/0001-6160(53)90126-6.
4. W.W. Mullins and R.F. Sekerka. J. Appl. Phys. **35**(2), 444 (1964). doi:10.1063/1.1713333.
5. J.W. Cahn. Acta Metall. **8**, 554 (1960). doi:10.1016/0001-6160(60)90110-3.
6. J.W. Cahn, W.B. Hillig, and G. Sears. Acta Metall. **12**, 1421 (1964). doi:10.1016/0001-6160(64)90130-0.
7. J.M. Ziman. Can. J. Phys. **35**, 1256 (1956). doi:10.1139/p56-139.
8. E.T. Jaynes. Phys. Rev. **108**(2), 171 (1957). doi:10.1103/PhysRev.108.171.
9. H. Ziegler. An introduction to thermomechanics. North Holland, Amsterdam. 1983.
10. H. Ziegler and C. Wehrli. J. Non-Equilib. Thermodyn. **12**, (3), 229 (1978). doi:10.1515/jnet.1987.12.3.229.
11. R. Dewar. J. Phys. A: Math. Gen. **36**, 631 (2003). doi:10.1088/0305-4470/36/3/303.
12. L.M. Martyushev and V.D. Seleznev. Phys. Rep. **426**, 1 (2006). doi:10.1016/j.physrep.2005.12.001.
13. R.A.W. Bradford. Phys. A, **392**, 6273 (2013). doi:10.1016/j.physa.2013.08.035.
14. S.A. Bruers. J. Phys. A: Math. Theor. **40**, 7441 (2007). doi:10.1088/1751-8113/40/27/003.
15. G. Grinstein and R. Linsker. J. Phys. A: Math. Theor. **40**, 9717 (2007). doi:10.1088/1751-8113/40/31/N01.
16. R.C. Dewar. Entropy, **11**, 931 (2009). doi:10.3390/e11040931.
17. N. Virgo. Entropy, **12**, 107 (2010). doi:10.3390/e12010107.

18. D. Kondepudi and I. Prigogine. Modern thermodynamics: from heat engines to dissipative structures. Wiley, New York. 1998.
19. H. Wang, F. Liu, H. Zhai, and K. Wang. Acta Mater. **60**, 1444 (2012). doi:10.1016/j.actamat.2011.11.038.
20. L.M. Martyushev and V.D. Seleznev. Phys. Rep. **426**, 1 (2006). doi:10.1016/j.physrep.2005.12.001.
21. A. Dobovišek, M. Vitas, M. Brumen, and A. Fajmut. BioSystems, **158**, 47 (2017). doi:10.1016/j.biosystems.2017.06.001.
22. A. Kleidon. Naturwissenschaften,. **96** 653 (2009). doi:10.1007/s00114-009-0509-x.
23. L.M. Martyushev, V.D. Seleznev, and I.E. Kuznetsova. Zh. Éksp. Teor. Fiz. **118**, **149** (2000). [In Russian.]
24. A. Hill. Nature, **348**, 426 (1990). doi:10.1038/348426a0.
25. Y.D. Bensah, H.P. Li, and J.A. Sekhar. Key. Eng. Mater. **521**, 79 (2012). doi:10.4028/www.scientific.net/KEM.521.79.
26. M.C. Flemings. Solidification processing. McGraw Hill, New York. 1974.

List of symbols

A_{SLI} area of the SLI (m^2)
C_p average heat capacity across the SLI (J m^{-3} K^{-1})
C_O solute concentration in the binary alloy material (mol m^{-3})
D_L diffusion coefficient of solute in a solvent (m^2 s^{-1})
ds_{CV}/dt total steady state entropy rate change in the control volume (J m^{-3} K^{-1} s^{-1})
f_s fraction solidified (dimensionless)
G_L temperature gradient in the liquid (K m^{-1})
G_S temperature gradient in the solid (K m^{-1})
G_{SLI} linear temperature gradient across the SLI (K m^{-1})
k partition coefficient (no units)
m_L slope of the liquidus line at the solid–liquid boundary for a binary material (K m^3 mol^{-1})
Q lost work potential from heat generation (J)
R volumetric gas constant (J m^{-3} K^{-1})
R_g molar gas constant (J mol^{-1} K^{-1})
$\dot{s}_E$ entropy generation rate density, which describes the new entropy generated due to exchange of matter at the SLI (J m^{-3} K^{-1})
$\dot{s}_{gen}$ irreversible entropy generation rate in the SLI region (J m^{-3} K^{-1} s^{-1})
$(S_{gen})_{HD}$ equivalent entropy generation through heat dissipation (J K^{-1})
$(S_{gen})_{max}$ maximum entropy generation due to the lost work (J K^{-1})
$\dot{s}_{in}$ rate of entropy entering the control volume (J m^{-3} K^{-1} s^{-1})
s_{LG} entropy generation density due to solute gradient in the liquid (J m^{-3} K^{-1})
$\dot{s}_{LG}$ entropy generation rate density by the solute gradient in the liquid (J m^{-3} K^{-1} s^{-1})
$\dot{s}_{out}$ rate of entropy leaving the control volume (J m^{-3} K^{-1} s^{-1})
s_{SG} entropy generation density due to solute gradient in the solid (J $m^{-3}K^{-1}$)
t time (s)
T_{av} average temperature between T_{li} and T_{si} across the SLI (K)
T_{li} liquidus temperature at the SLI boundary (K)
T_M melting temperature (K)
T_{si} solidus temperature at the SLI boundary (K)
V solidification growth velocity (m s^{-1})
W_L lost work (J)
δ_C solute boundary layer (m)
Δh_{sl} heat of fusion (J m^{-3})
Δh_m heat of fusion of the solid with defects (J m^{-3})
ΔS_{sl} entropy change during solidification per unit volume (J m^{-3} K^{-1})
ΔT_O solidification temperature range (K)
$\Delta\rho_k$ overall density shrinkage (kg m^{-3})
$\Delta\rho$ density change from liquid to solid (kg m^{-3})
$\Delta\Omega_S$ volume shrinkage associated with the liquid to solid transformation (m^3)
ρ_l density of the rigorous liquid (kg m^{-3})
ρ_s density of the rigorous solid (kg m^{-3})
$\dot{\varphi}_{max}$ maximum entropy generation rate density, which is a measure of MEPR at the SLI (J m^{-3} K^{-1} s^{-1})
ω_D energy of defects (J m^{-3})

Appendix A: Derivation of the entropy generation from the solute gradient in the liquid

For steady state conditions, the solute flux J_s (mol s^{-1}) in the liquid entering the interface for a given flux area A_f (m^2) is related to Fick's first law of diffusion [26] as

$$J_s = -A_f D_L\left(\frac{dC_{LG}}{dz}\right) \tag{A1}$$

where dC_{LG}/dz (mol m^{-4}) is the change in solute gradient in the liquid, dz (m) is the change in the position length of the solute, and dC_{LG} (mol m^{-3}) is the change in concentration at a distance, z, from the interface. The solute gradient in the liquid can be replaced with $-\Delta C_O/\delta_C$ [26] where δ_C (m) is the diffusion boundary layer and the negative sign represents the depletion of solute along the distance, z. Entropy is also generated when the solute in the liquid travels across the interface to form a solid through an established solute gradient. The driving force $\Delta\mu_c$ (J mol^{-1}) associated with the solute gradient is given as

$$\Delta\mu_C = R_g T_m \ln\left(\frac{1}{k}\right) \tag{A2}$$

Although k is non-dimensional, the numerical value depends on the concentration units chosen. However, for the entropy generation calculations this is multiplied by the composition difference. It is also recognized that, when comparing interface configurations for stability, the value of k for a DI-based configuration will be different than that when the interface has an atomistically smooth topography. Multiplying (A1) by (A2) and diving by the melting temperature T_m (K) of the material gives the flux entropy rate S_f (J $K^{-1}s^{-1}$) as

$$S_f = A_f D_L R_g\left(\frac{\Delta C_O}{\delta_C}\right)\ln\left(\frac{1}{k}\right) \tag{A3}$$

The change in solute gradient in the liquid ΔC_O (mol m^{-3}), the flux volume Ω_f (m^3), and the diffusion boundary layer δ_C (m) are given as

$$\Delta C_O = \frac{\Delta T_O}{m_L} \tag{A4}$$

$$\Omega_f = A_f\delta_C \tag{A5}$$

where m_L (K m^3 mol^{-1}) is the slope of the equilibrium liquidus line at the solid–liquid boundary for a binary material obtained from the phase diagram. Now rearranging (A2) and (5) into (A3) and dividing by (A5) gives the entropy rate density, which describes the force-flux entropy generated by the existence (support) of maintaining the solute gradient as

$$\dot{s}_{LG} = \frac{\Delta T_O}{D_L}\frac{V^2 R_g \ln(1/k)}{4m_L} \tag{A6}$$

which is (4) in the text.

For the entropy generation inside the boundaries of the solid–liquid zone this gradient entropy reduces the total amount of the irreversible entropy generated as may be noted from (7).